Ion density evolution in a high-power sputtering discharge with bipolar pulsing

N. Britun,[1] M. Michiels,[1,2] T. Godfroid,[2] and R. Snyders[1,2]

[1]*Chimie des Interactions Plasma-Surface (ChIPS), CIRMAP, Université de Mons, 23 Place du Parc, B-7000 Mons, Belgium*
[2]*Materia Nova Research Center, Parc Initialis, B-7000 Mons, Belgium*

Time evolution of sputtered metal ions in high power impulse magnetron sputtering (HiPIMS) discharge with a positive voltage pulse applied after a negative one (regime called "bipolar pulse HiPIMS"—BPH) is studied using 2-D density mapping. It is demonstrated that the ion propagation dynamics is mainly affected by the amplitude and duration of the positive pulse. Such effects as ion repulsion from the cathode and the ionization zone shrinkage due to electron drift towards the cathode are clearly observed during the positive pulse. The BPH mode also alters the film crystallo-graphic structure, as observed from X-ray diffraction analysis. *Published by AIP Publishing.*
https://doi.org/10.1063/1.5030697

Extraction, transport, and deposition of atoms or mole-cules on a solid surface have undergone essential develop-ment after the introduction of direct current magnetron sputtering (DCMS) in the early 1960s,[1] followed by pulsed DCMS, and finally high power impulse magnetron sputtering (HiPIMS) in the 1990s.[2] The main benefit of the latter dis-charge family is the elevated ionization degree attained by applying high power levels (up to $\sim$100 kW) during short pulses (up to few hundreds μs).[3] High discharge ionization and efficient ion acceleration towards a growing film were always the key factors for film deposition by sputtering, as the accelerated ions bring additional energy to the film sur-face, changing its properties.[4] In this way, a high ionization degree of HiPIMS discharges combined with substrate bias-ing should be especially beneficial for reliable industry-grade film structure control.

Biasing the film substrate may often be an impossible or at least a very challenging task. This brought researchers to the idea of using a second voltage pulse with the opposite polarity, or simply "bipolar pulsing" (notation used in this work) which would accelerate plasma-produced ions away from the cathode. Since in most of the cases, sputtering is realized by positive ions (often Ar^+) when the cathode is biased negatively, and the second pulse must have positive polarity. Evidently, as far as a single cathode is used, two pulses must be separated in time and properly synchronized for optimum performance.

Several ideas on biasing the magnetron cathode for the sake of increasing ion energy after the plasma pulse in the HiPIMS case emerged in the 2000s.[5–7] Later on, the influence of a positive cathode bias applied during the *entire* plasma off-time on the discharge current evolution has been studied by Nakano *et al.*[8] However, synchronized ion repulsion has been proposed in this work. The idea of the bipolar discharge regime with a negative (plasma) pulse and a *controllable* pos-itive (bias) pulse in the HiPIMS case (referred in this work as "bipolar pulse HiPIMS" or BPH) is implemented only in 2018 by Wu *et al.*,[9] where a beneficial effect of bipolar puls-ing on the Cu film stress and adhesion is shown.

The fundamental plasma processes in the BPH dis-charges, such as the electron and ion density evolution, remain unexplored, even though the overall advantages of the bipolar mode for film deposition were clearly demon-strated in the previous works. On the other hand, knowledge of the particle density dynamics in the discharge leads to a basic understanding of its properties and discharge physics and may result in potential discharge improvements. Thus, in order to elucidate the details of particle motion in the BPH discharges, this letter represents an attempt of studying the ion dynamics in BPH discharge by two-dimensional time-resolved ion density mapping.

In our study, a balanced magnetron source placed in a vac-uum chamber with a base pressure of $\sim$10^{-6} Pa and connected to a Lab-made BPH power supply has been used, as shown in Fig. 1(a). A sketch of the electric (**E**) and magnetic (**B**) field strength lines of the mentioned source along with the 65 mm high and 95 mm wide region of interest (ROI) used for density imaging are shown in Fig. 1(b). A Ti round flat cathode (10 cm in diameter and 1 cm thick) has been used. The B value in the cathode center near its surface was about 0.1 T. For the sputter-ing process, the chamber was filled by Ar at 0.7 Pa. The BPH power supply is based on a half-bridge electronic module con-verting a conventional DCMS system to a HiPIMS system in which a classical negative pulse followed by a delayed positive pulse is implemented (with controllable duration, amplitude, and delay between them). The discharge current has been mea-sured using a 1 MHz bandwidth Tektronix TCP303 current probe with a TCPA300 amplifier connected to a Tektronix DPO3054 digital oscilloscope. The current sign is accepted negative during the negative voltage pulse (and vice versa) for the sake of notation consistency. The plasma pulse repetition rate was f = 300 Hz (unless stated otherwise). The typical BPH voltage and current waveforms with the used notations are shown in Fig. 2(a). The bipolar regime was typically repre-sented by a 20 μs negative pulse (V$_-$ varied from -500 to -700 V) following (after a $\tau_\pm = 10\,\mu$s delay) by a positive pulse with the length $\tau_+ = 250\,\mu$s and voltage V$_+$ varied from 0 to $+300$ V. The time-averaged discharge power value was
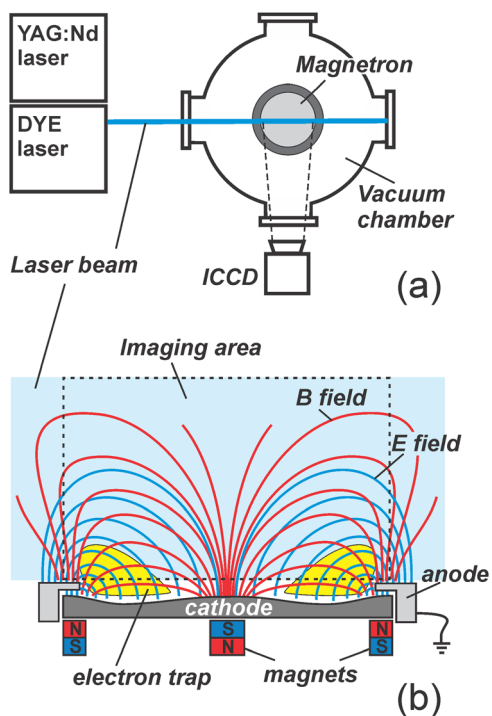
FIG. 1. (a) Top view of the experimental setup including the pulsed laser and vacuum chamber with a magnetron source. (b) Side view of the magnetron source with sketched magnetic and electric field strength lines. The laser beam direction is from left to right (also in the figures below).

FIG. 2. General current and voltage waveforms in the BPH case (a), along with the influence of V_+ (b), $\tau_\pm$ (c), τ_- (d), and I_-^p (e) on the I_+ current shape during the positive voltage pulse. In the case of (e), f = 80 Hz.

typically ∼40 W. The peak discharge current (I_-^p) has been varied from 15 A to 70 A. High I_-^p values were rarely used, especially in the case of the time consuming laser-based measurements in order to avoid heating of the magnetron cathode and the BHP power supply circuitry. The high-current measurements did not show any abrupt qualitative differences in the ion density distribution compared to the low current case (shown below) and thus did not affect the main conclusions made in this work.

Time-resolved evolution of the Ti^+ density has been studied by laser-induced fluorescence (LIF) imaging. Excitation of the ground state Ti ions has been realized at $\lambda_{air} = 314.804$ nm by a pulsed Sirah dye laser working at 10 Hz and 5 ns of pulse duration.[10] The fluorescence signal was detected using an Andor intensified charge coupled device (ICCD) camera with a Nikkor 50 mm f/1.4 lens via an optical 460/10 nm bandpass filter. The accumulating mode of the ICCD (150 laser pulses) and the optical gate of 50 ns have been used. The laser system and the BPH discharge were synchronized by transistor-transistor logic (TTL) signals using a DG645 digital delay generator.

Classical HiPIMS (i.e., non-BPH) process is typically characterized by several important stages including the acceleration of positive ions remaining from the previous plasma pulse towards the negative cathode (at the beginning of the plasma pulse), ionization of Ar and acceleration of Ar^+ towards the cathode, sputtering itself accompanying by secondary electron ejection from the cathode surface,[3] electron capturing in the magnetic trap [see Fig. 1(b)], propagation [with a velocity of ∼10³ m/s (Ref. 11)] and ionization (mainly in the electron trap[12]) of the sputtered atoms,
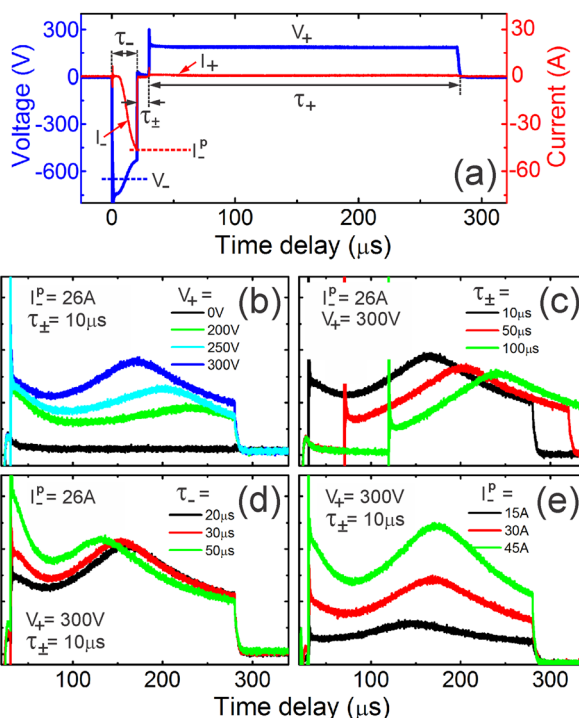
followed by their gradual diffusion and thermalization till the end of the off-time.[10] In the Ar-Ti case, the discharge current in the non-reactive regime is mainly formed by the Ar^+ and Ti^+ ions hitting the negative cathode.[13] It decays nearly exponentially after the plasma pulse.[3] In our case, due to the short plasma pulse used ($<50\,\mu s$), the discharge current saturation[3] is not visible and current has a nearly triangular shape before reaching its peak value I_-^p [see Fig. 2(a)].

We found that in the BPH mode, after positive voltage is applied, the discharge current reveals a reversed component (called here I_+) during the positive pulse, as shown in Figs. 2(b)–2(e). This current does not exceed about 5% of the I_-^p value and is supposed to be formed by the negative charge carriers since the cathode is charged positively. The electrons produced above the cathode during the plasma phase are the main candidates for such carriers, along with the negatively charged ions whose contribution might be essential in electro-negative discharges (not in the Ar-Ti case, though).

The measured I_+ current evolution reveals two peaks [Figs. 2(b)–2(e)], one adjacent to the growing front of the positive pulse, followed by a wider one, depending both on V_+ [Fig. 2(b)] and I_-^p [Fig. 2(e)]. In the last case, the I_+ current waveform shape remains similar also at higher I_-^p values, showing a proportional increase in I_+ amplitude and similar timing for the second I_+ peak [I_-^p values up to 70 A were used, not shown in Fig. 2(e)]. An overall increase in the I_+ current value with V_+ (or/and I_-^p) points out a higher amount of electrons attracted by the cathode (or/and produced in the plasma pulse) during the positive pulse. At the same time, the first I_+ peak is barely sensitive to V_+ [Fig. 2(b)] but sensitive to I_-^p [Fig. 2(e)], additionally confirming

this suggestion. Both I_+ peaks stand on a non-zero current base, which gradually decays and saturates to a certain value under long enough τ_+ time (verified up to few ms) and can be associated with the non-trapped electrons gradually pulled by the positive cathode during plasma off-time.

Furthermore, the first I_+ peak value increases at longer τ_- values [Fig. 2(d)] since more electrons are produced during longer plasma pulses. On the other hand, its value decreases at longer $\tau_\pm$ delays [Fig. 2(c)] as the produced electrons have more time to diffuse away from the *neutral* cathode before the arrival of the positive pulse. We believe that this peak is formed by the electrons produced at the very end of the plasma pulse which are located near the cathode surface at the moment of switching cathode polarity. In this way, the I_+ current shape should follow the I_- current at the end of the plasma pulse (reversed in time, though). The I_+ current is supposed to be mainly formed by the electrons produced as a result of Ar/Ti ionization with a small addition of secondary electrons ejected from the cathode. The fraction of secondary electrons contributing to the discharge current does not exceed 1 percent in the non-reactive HiPIMS case,[14] as found in the recent modeling work of Gudmundsson *et al.*[13] Let us note that the role of these electrons can be yet smaller under domination of Ti ion sputtering over Ar ion sputtering, as the secondary electron emission yield is ~0 for Ti$^+$.[15] For short plasma pulse durations ($\tau_- \sim 50\,\mu s$ or less), however, Ar ion sputtering can be safely assumed.[13]

The wide I_+ current peak found in our case likely represents the contribution of the electrons confined in the magnetic trap, i.e., far from the cathode, requiring longer time to reach the cathode surface. This peak appears earlier at higher V_+ [Fig. 2(b)], gets shifted proportionally to $\tau_\pm$ delay time [Fig. 2(c)], and remains barely affected by the plasma pulse duration τ_- [Fig. 2(d)]. The first two observations are supposed to be the result of rather slow electron trap depletion (~$100\,\mu s$ in the non-BPH case[10]), whereas the last one remains unclear for now.

Most of the described current effects are in agreement with the LIF imaging results shown in Fig. 3, where the Ti$^+$ ground state density distributions measured during the plasma off-time are presented. In the non-BPH case [Fig. 3(a)], the ion density evolution is defined by the propagation of the sputtered metal atoms, their ionization in the electron trap, followed by gradual diffusion and thermalization, as studied recently.[10] Additional optical absorption measurements[16,17] give a value of ~5×10^{16} m^{-3} for Ti$^+$ ground state density at $150\,\mu s$.

Two other cases [Figs. 3(b) and 3(c)] correspond to the BPH regime at different V_+ voltages applied. Quite different processes are visible here, such as the shrinkage of the ionization zone [in the electron trap vicinity, see Fig. 1(b)] and the ion propagation upwards, leading to an abrupt ion density decay at the end of the positive pulse. As we can see, at $40\,\mu s$, Ti$^+$ density distributions look similar, as the ions react slowly to the E-field induced by the positive pulse due to their inertia and collisions. The ion density maps become quite different only after $100\,\mu s$ underlying the importance of positive pulse duration for efficient ion repulsion. The vertical ion propagation is clearly observed in the BPH mode [e.g., at 120–$150\,\mu s$ in Fig. 3(c)]. We can also see that the higher V_+ values
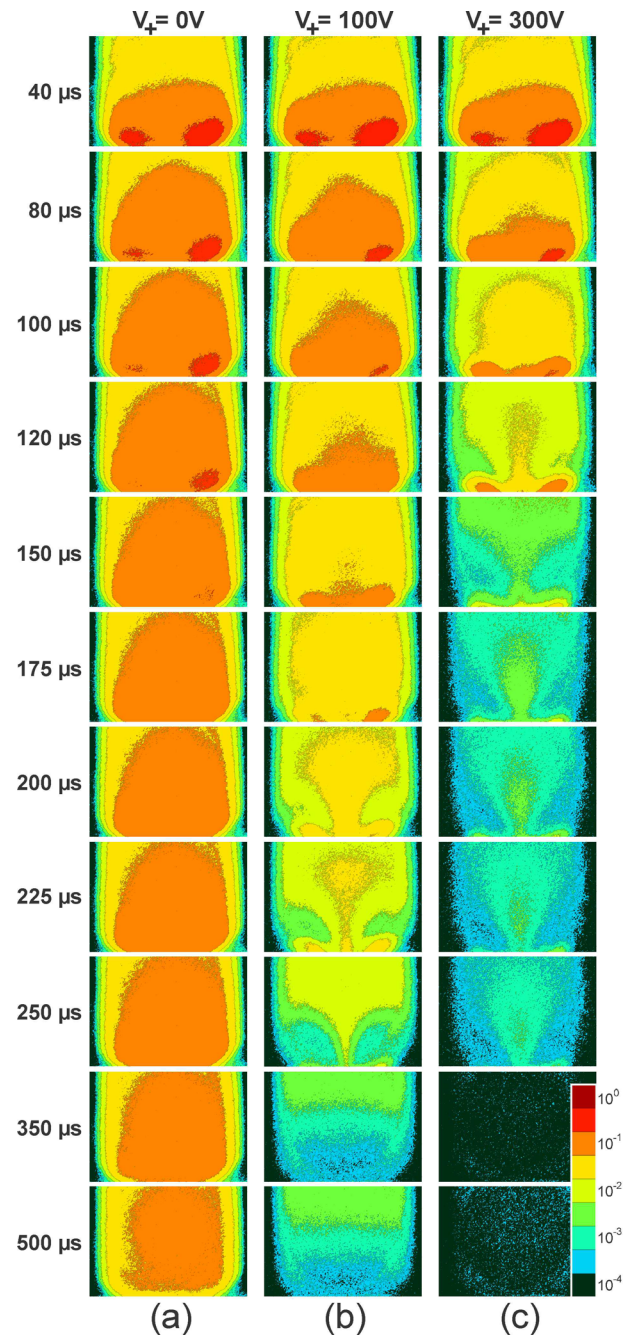
FIG. 3. Time-resolved Ti$^+$ ground state density evolution above the cathode at $V_+ = 0$ V (a), 100 V (b), and 300 V (c). $I_-^p = 26$ A, f = 300 Hz, $\tau_- = 20$ μs, and $\tau_\pm = 10\,\mu s$. The delay time starting from the plasma pulse beginning is shown on the left. All images are normalized to one value. Logarithmic color space is used.

correspond to faster ion acceleration and faster density redistribution, as the ion density tail (observed at $250\,\mu s$ at $V_+ = 100$ V) appears ~$100\,\mu s$ earlier at $V_+ = 300$ V. The overall density decays by 1–2 orders of magnitude during the positive pulse, compared to the non-BPH case. Most likely, it is the result of widening of the ion velocity distribution function in the vertical direction, which happens due to ion acceleration (the laser linewidth remains constant). Note that such widening is negligible in the horizontal direction (as shown below).

The observed non-uniformity of Ti$^+$ density distribution is also defined by the **E** and **B** field topology [see Fig. 1(b)]. In the BPH mode, the ionization zone shrinks during the
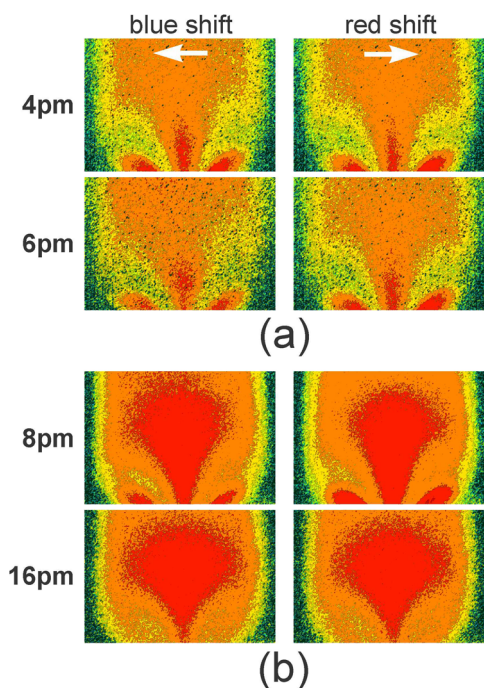
FIG. 4. DS-LIF density maps corresponding to several Ti^+ horizontal velocity groups. The absolute value of the laser wavelength shift is indicated aside. (a) $I_-^p = 26$ A, $V_+ = 100$ V, f = 300 Hz, and delay = 220 μs. (b) $I_-^p = 70$ A, $V_+ = 300$ V, f = 80 Hz, and delay = 130 μs. 1 pm corresponds to ~ 0.95 km/s. $\tau_- = 20\,\mu$s and $\tau_+ = 10\,\mu$s. Each image is normalized separately. The color scheme from Fig. 3 is used.

positive pulse as electrons leave the trap (where $\mathbf{E} \perp \mathbf{B}$) downwards. This effect is absent in Fig. 3(a) but clearly visible in Figs. 3(b) and 3(c) correlating well with the I_+ current evolution shown in Fig. 2, namely, with the appearance of the wide I_+ peak at $\sim 170\,\mu$s (at $V_+ = 300$ V). In addition, Ti^+ density gets clearly rarefied *above* the electron trap (i.e., where $\mathbf{E}$ and $\mathbf{B}$ are nearly parallel) as the positive pulse evolves, e.g., after 120 μs in Fig. 3(c). The combination of ion drift and the drift of the non-trapped electrons in the $\mathbf{E}$ field, leading to a decrease in Ti ionization, may be the reasons for this effect. Ion gyration in the $\mathbf{B}$ field resulting in an ion deviation from the imaging plane might be another reason and however rather negligible, as the Larmor radius for ions lies in the cm range in our case.

The contribution of ion drift in the horizontal direction during the positive pulse can be deduced from the Doppler-shift LIF (DS-LIF) analysis shown in Fig. 4, where several groups of blue- and red- shifted Ti ions are selectively visualized depending on their horizontal velocity (by shifting the laser wavelength). As we can see, the ion density distributions for either blue- or red- shifted ions look very similar. Thus, the ions can be assumed thermalized horizontally, as the asymmetry of the blue- and red-shifted maps is minimal and also because the high-speed ion populations (Doppler shift > 8 pm) represent only few per cent of the total population in the ROI, as verified separately. It is also interesting that the ions with very high horizontal speed are not present in the electron trap area [see Fig. 4(b) at 16 pm shift], implying narrow ion energy distribution in the horizontal direction in this region. The Ti^+ density depletion above the electron trap mentioned above may also be caused by the drift of
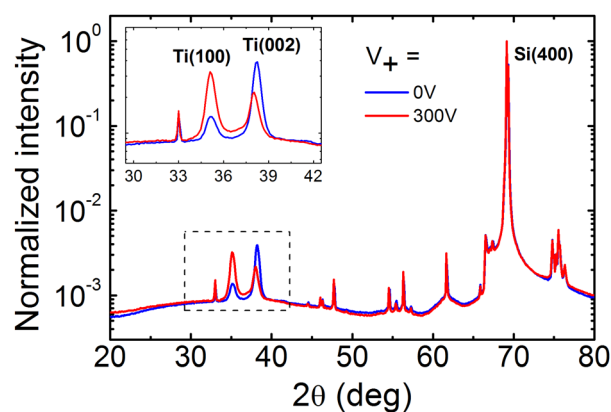
FIG. 5. Normalized XRD patterns corresponding to two ~ 100 nm Ti films deposited on a Si substrate without and with the BPH effect (at $V_+ = 300$ V). $I_-^p = 70$ A and f = 80 Hz.

non-trapped electrons in the $\mathbf{E}$ field during the positive pulse. This effect, however, requires additional electron density measurements being out of scope of this letter.

Finally, we have verified the effect of the BPH mode on the film structure using X-ray diffraction (XRD) analysis, as shown in Fig. 5. These results show that in the BPH mode, the crystallographic orientation of the deposited Ti films changes form the (002) to (100) plane dominance. Such changes are typical for the DCMS to HiPIMS process transition, reflecting the influence of a higher ion density in the HiPIMS case.[18] Similar changes found in our case approve the ion influence in the BPH mode, altering the film structure in the same way. At the same time, the XRD line broadening remains nearly unaffected, implying negligible changes in the average grain size.

As a conclusion, several characteristic features of ion density behavior in the BPH discharge regime were found. The most important of them are the shrinkage of the ionization zone near the cathode, ion acceleration away from the cathode, the presence of the time-dependent reversed current (I_+) during the positive pulse, and general ion density re-distribution induced by the $\mathbf{E}$ and $\mathbf{B}$ field configuration near the cathode. Being well-thermalized in the horizontal direction, the discharge ions undergo significant acceleration vertically (in our geometry) which results in their apparent density drop, as a result of widening of the velocity/energy distribution function. The last statement is a subject of further experimental work in which the mass spectrometry analysis, further optimization of the BPH discharge, and investigations related to the film structure should be involved.

[1] E. Kay, J. Appl. Phys. **34**, 760 (1963).
[2] D. V. Mozgrin, I. K. Fetisov, and G. V. Khodachenko, Plasma Phys. Rep. **21**, 400 (1995).
[3] J. T. Gudmundsson, N. Brenning, D. Lundin, and U. Helmersson, J. Vac. Sci. Technol. A: Vac., Surf., Films **30**, 030801 (2012).
[4] U. Helmersson, M. Lattemann, J. Bohlmark, A. P. Ehiasarian, and J. T. Gudmundsson, Thin Solid Films **513**, 1 (2006).

⁵S. Konstantinidis, J. P. Dauchot, M. Ganciu, A. Ricard, and M. Hecq, J. Appl. Phys. **99**, 013307 (2006).

⁶P. Vasina, M. Mesko, J. C. Imbert, M. Ganciu, C. Boisse-Laporte, L. de Poucques, D. P. M. Touzeau, and J. Bretagne, Plasma Source Sci. Technol. **16**, 501 (2007).

⁷J. Lin, J. J. Moore, B. Mishra, M. Pinkas, W. D. Sproul, and J. A. Rees, Surf. Coat. Technol. **202**, 1418 (2008).

⁸T. Nakano, C. Murata, and S. Baba, Vacuum **84**, 1368 (2010).

⁹B. Wu, I. Haehnlein, I. Shchelkanov, J. McLain, D. Patel, J. Uhlig, B. Jurczyk, Y. Leng, and D. N. Ruzic, Vacuum **150**, 216 (2018).

¹⁰N. Britun, M. Palmucci, S. Konstantinidis, and R. Snyders, J. Appl. Phys. **117**, 163302 (2015).

¹¹N. Britun, J. G. Han, and S. G. Oh, Appl. Phys. Lett. **92**, 141503 (2008).

¹²C. Huo, M. A. Raadu, D. Lundin, J. T. Gudmundsson, A. Anders, and N. Brenning, Plasma Source Sci. Technol. **21**, 045004 (2012).

¹³J. T. Gudmundsson, D. Lundin, N. Brenning, M. A. Raadu, C. Huo, and T. M. Minea, Plasma Source Sci. Technol. **25**, 065004 (2016).

¹⁴J. T. Gudmundsson and D. Lundin, private communication (May 24, 2018).

¹⁵N. Brenning, J. Gudmundsson, M. A. Raadu, T. J. Petty, T. Minea, and D. Lundin, Plasma Sources Sci. Technol. **26**, 125003 (2017).

¹⁶N. Britun, M. Palmucci, S. Konstantinidis, and R. Snyders, J. Appl. Phys. **117**, 163303 (2015).

¹⁷N. Britun, M. Michiels, and R. Snyders, Rev. Sci. Instrum. **86**, 123114 (2015).

¹⁸F. J. Jing, T. L. Yin, K. Yukimura, H. Sun, Y. X. Leng, and N. Huang, Vacuum **86**, 2114 (2012).